Passive *Q*-switching in an erbium-doped fiber laser using tungsten sulphoselenide as a saturable absorber

H. Ahmad*, Z. C. Tiu, and S. I. Ooi

Photonics Research Centre, University of Malaya, Kuala Lumpur 50603, Malaysia
**Corresponding author: harith@um.edu.my*

Received October 30, 2017; accepted December 22, 2017; posted online January 31, 2018

A highly stable *Q*-switched laser incorporating a mechanically exfoliated tungsten sulphoselenide (WSSe) thin sheet saturable absorber (SA) is proposed and demonstrated. The SA assembly, formed by sandwiching a thin WSSe sheet between two fiber ferrules within the erbium-doped fiber laser, is used to effectively modulate the laser cavity losses. The WSSe-based SA has a saturation intensity of ~0.006 MW/cm^2 and a modulation depth of 7.8%, giving an optimum *Q*-switched laser output with a maximum repetition rate of 61.81 kHz and a minimum pulse width of 2.6 μs. The laser's highest output power of 0.45 mW and highest pulse energy of 7.31 nJ are achieved at the maximum pump power of 280.5 mW. The tunability of the cavity's output at the maximum pump power is analyzed with a C-band tunable bandpass filter, giving a broad tunable range of ~40 nm, from 1530 nm to 1570 nm. The output performance of the tunable *Q*-switched laser correlates well with the gain spectrum of erbium-doped fibers, with the shift in the gain profile as a result of the saturated SA.

OCIS codes: 140.3500, 140.3510, 140.3540, 140.3600.
doi: 10.3788/COL201816.020009.

In recent years, two-dimensional (2D) semiconductor materials such as graphene[1], transition metal dichalcogenides (TMDs)[2], and topological insulators (TIs)[3] have received significant attention for various applications in the field of photonics and optoelectronics. These materials find a use as saturable absorbers (SAs) for the passive generation of pulsed laser outputs due to their low saturation intensity, ultrafast carrier dynamics, as well as great photoluminescence of 2D materials[4]. The ability of 2D materials to modulate intracavity losses in a fiber laser system contributes to their successful incorporation in various *Q*-switching and mode-locking systems[1,2]. Specifically, TMDs have seen more applications in *Q*-switching and mode-locking systems compared to other 2D materials due to their better performance as well as their layer-dependent absorption properties, which gives TMDs an advantage over most other 2D materials.

TMD materials are generally represented by the formula MX_2, where M represents the transition metal atom and X represents the chalcogen atom[5]. Within the TMD layer, the two X atoms hold onto each M atom by a strong covalent bond, while only a weak van der Waals force holds the TMD layers to each other. The weak interlayer forces of TMDs make them easy to fabricate into a single or few layer form using simple exfoliation methods[6]. Furthermore, by changing the number of layers in these TMD materials, the energy bandgap can be tuned from indirect to direct feature[7]. This tuning ability, combined with high third-order optical nonlinearities, and ultrafast carrier dynamics give TMDs a high potential for various broadband absorber photonics and optoelectronics applications. In particular MoS_2, $MoSe_2$, WS_2, and WSe_2 have shown a tremendous potential for use as SAs in photonics applications.

Recently, breakthroughs in the preparation and fabrication process of TMDs for SA applications have been able to further enhance their optical properties. The improvements in the sample preparation process have lead to the existence of TMD alloys with the chemical formula $MX_{2(1-x)}X'_{2x}$, where x represents the composition ratio[8]. This new category of TMD alloys has a bandgap tuning range over the absorption wavelength that is dependent on the composition ratio x[8]. Furthermore, these TMDs are very stable due to their ordered alloy structures[9]. Owing to their attractive output characteristics, TMD alloys have been studied in previous works[10], but to date there has been no known exploration of the feasibility of the $WS_{2(1-x)}Se_{2x}$ alloy as an SA.

In this work, a van der Waals heterostructure-based $WS_{2(1-x)}Se_{2x}$ composite SA with a composition ratio of 0.5 is fabricated from a bulk crystal by simple mechanical exfoliation. The exfoliated few-layer WSSe SA is then incorporated into an erbium-doped fiber laser (EDFL) cavity operating at 1.56 μm. From the nonlinear optical characterization of the WSSe SA by the twin-detection technique, a saturation intensity of 0.006 MW/cm^2 and a modulation depth of ~7.80% were observed. The ability of the WSSe SA to modulate intracavity losses results in the passive generation of *Q*-switched pulses in the proposed EDFL cavity.

A sample of the mechanically exfoliated few-layer WSSe crystal is first characterized by X-ray diffraction (XRD) using a PANalytical EMPYREAN X-ray diffractometer. Figure 1 shows the detailed XRD patterns of the characterized WSSe sample at an excitation wavelength of 1.5406 Å. The WSSe sample shows diffraction peaks at 13.80°, 29.15°, 38.76°, 42.80°, 48.60°, and 57.84° along (002), (004), (103), (006), (105), and (110),

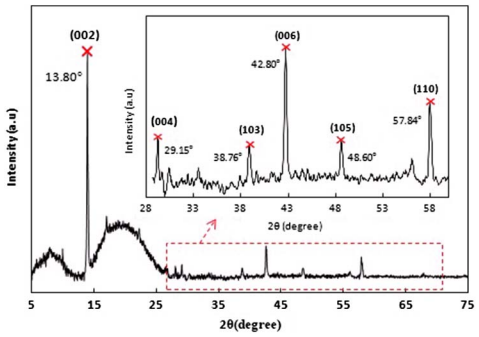

Fig. 1. XRD patterns of WSSe-exfoliated crystal.

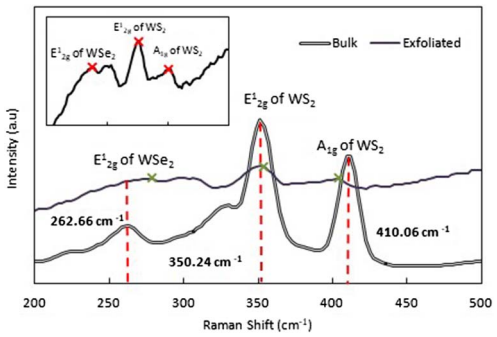

Fig. 3. Raman spectra of the bulk and exfoliated WSSe crystal. The inset shows the Raman spectrum of the exfoliated WSSe crystal with its peaks made easier to see.

respectively. The obtained diffraction peaks in the tested WSSe sample are all slightly smaller than the standard values, with the difference in the angle of diffraction peaks indicating the existence of strain and large interlayer spacing in the tested sample[11]. Furthermore, field emission scanning electron microscope (FESEM) characterization was also performed using a Hitachi SU8220 FESEM. Figures 2(a) and 2(b) show, respectively, the morphological structure and elemental composition of the WSSe sample. From the FESEM scan, the layer structure of the exfoliated crystal can be seen, especially at the edges of each separated flake. Figure 2(b) confirms the presence of all the expected elements in the analyzed sample through the energy-dispersive X-ray (EDX) analysis. From the results obtained, the W element shows the highest composition at approximately 36.95% of the total, with the other two chalcogen atoms comprising 31.16% for the element S and 31.90% for the element Se, respectively. The ratio of S and Se is quite balanced, indicating an x value of 0.5 in the tested sample. Thus, all the necessary elements in the tested sample are at significant composition ratios, confirming the presence of the W, S, and Se elements.

Raman spectrum characterization was also performed on both the bulk and exfoliated WSSe samples using a Renishaw inVia Raman spectroscope at an excitation wavelength of 514 nm. Figure 3 shows the Raman spectra of both the bulk and exfoliated WSSe samples, with the bulk WSSe sample showing three peaks at 262.66, 350.24, and 410.06 cm^{-1}, respectively. The three peaks represent the E^1_{2g} modes of WSe_2 as well as the E^1_{2g} and A_{1g} modes of WS_2, respectively, which is indicated in Fig. 3. In the exfoliated sample, on the other hand, the three peaks shift to 274.33, 350.94, and 405.60 cm^{-1}, respectively. The upshift of the A_{1g} mode in WS_2 is due to the lattice stiffening effect expected when additional layers are added. On the other hand, the downshift of the E^1_{2g} modes in both WS_2 and WSe_2 is attributed to the softening of the lattice as the number of layers increases. From the shift of the A_{1g} mode and the E^1_{2g} mode, the exfoliated WSSe is estimated at 5 to 8 layers[12].

Figure 4 shows the nonlinear absorption curve of the mechanically exfoliated WSSe sample characterized by the twin detector method. In the analysis, a mode-locked cavity operating at 1560 nm with a repetition rate of 27.933 MHz and a pulse width of 2.46 ps is used as the seed pulse. Characterization of the sample gives a saturation intensity of ~ 0.006 MW/cm^2 with a saturable absorption or modulation depth of ~7.8%. The nonsaturable absorption achieved is ~92%. The high nonsaturable absorption loss might be attributed to the relatively high insertion loss and minor scattering of the WSSe at 1560 nm. However, the nonsaturable absorption obtained from this work is comparable to that achieved in some previous work by others using MoS_2[13] and carbon nanotubes[14].

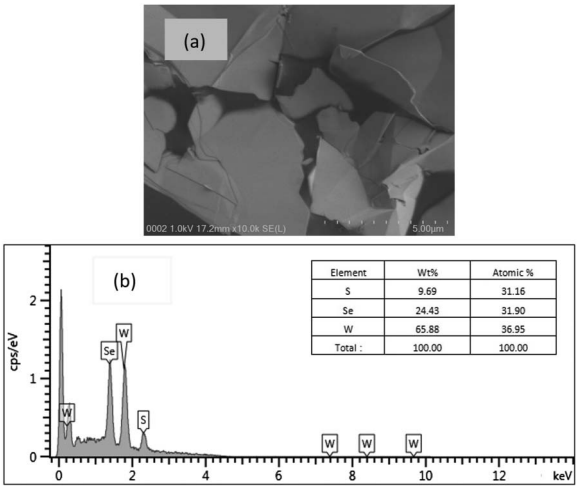

Fig. 2. (a) FESEM image of the exfoliated WSSe sample and (b) the elemental composition of the exfoliated WSSe sample.

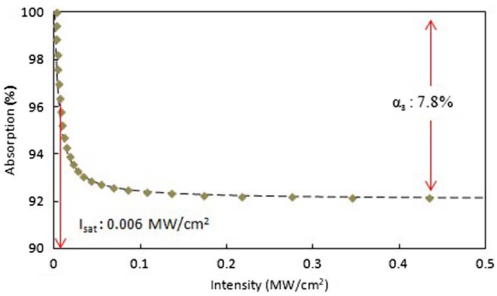

Fig. 4. Nonlinear absorption characterization of the WSSe-exfoliated crystal using the twin detection technique.

The setup of the C-band Q-switched EDFL is given in Fig. 5. A 974 nm laser diode (LD) with a maximum pump power of ~300 mW is used as the pump source for the laser cavity. The pump laser is injected into a 50 cm long erbium-doped fiber (EDF) through the 980 nm port of a 980/1550 nm wavelength division multiplexer (WDM). The EDF used has a dopant concentration of 2000 ppm, an absorption rate of 16.0 dB/m at 1530 nm, a mode field diameter of 9.5 μm at 1550 nm, and a numerical aperture of 0.13. In order to ensure the unidirectional propagation of intracavity light, a polarization insensitive (PI) isolator is placed in the cavity immediately after the gain medium. When pumped by the LD, the emission from the EDF is directed through the PI isolator and into the SA assembly, which is formed by simply sandwiching a small piece of the few-layer WSSe sample in between two fiber ferrules. The mechanically exfoliated $WS_{2(1-x)}Se_{2x}$ alloy used in this particular work has a composition ratio of $x = 0.5$ and is used to induce Q-switching in the cavity. A tunable bandpass filter is also inserted after the SA assembly for wavelength-dependence analysis of the laser cavity's output. Last, a 90/10 output tap coupler is used to extract 10% of the intracavity signal for analysis purposes, with the 90% port of the coupler being linked to the 1550 nm port of the WDM, thus completing the optical circuit. Analysis of the laser's output is done in the spatial, temporal, and frequency domains using a Yokogawa AQ6370B optical spectrum analyzer (OSA) at a resolution of 0.02 nm, a Yokogawa DLM2054 2.5GS/s-500MHz oscilloscope (OSC), and an Anritsu MS2683A radio frequency spectrum analyzer (RFSA) with a resolution of 300 Hz, respectively.

Continuous wave (CW) lasing occurs from a lasing threshold of approximately 15.18 mW, while Q-switching starts at a threshold power of ~89.07 mW. The Q-switching is observed to be stable from its threshold power up to the maximum pump power of 280.5 mW. Figure 6 shows the change in the spatial domain of the lasing output as the laser transfers from the CW to the pulsed regimes. A wavelength shift of ~10 nm and spectrum broadening of ~0.8 nm are observed as the lasing output transits between the two regimes. The CW lasing wavelength, obtained when the WSSe-based SA is absent from the cavity, is centered at 1568.4 nm. Incorporating the WSSe SA will induce a loss in the system, causing the lasing wavelength to be blueshifted toward the higher gain region to compensate for the incurred loss due to the SA. This results in a new lasing wavelength at 1558.4 nm. Similarly, the full width at half-maximum (FWHM) of the CW laser is narrow, about 0.5 nm, before expanded to 1.3 nm as the laser transits into the Q-switching regime. The central wavelength blueshift is a result of the gain profile of the EDFL shifting to compensate for the additional loss induced by the SA, while the broadening of the lasing wavelength's FWHM is a result of the self-phase modulation (SPM) effect at high pump powers.

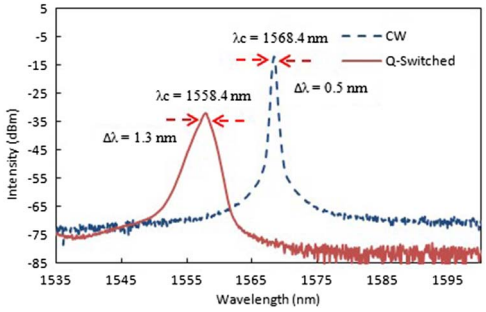

Fig. 6. Optical output of EDFL with and without incorporation of the WSSe SA.

Figure 7 indicates the three-dimensional (3D) pulse train evolution of the Q-switched laser over the entire Q-switching operation pump power range, from 89.07 mW to 280.5 mW. From the figure, it can be seen that no Q-switched pulses are observed at pump powers below 89.07 mW, as at this point there is still insufficient pump power to induce saturation in both the gain medium and the SA. On the other hand, at the maximum pump power, the maximum repetition rate is observed as well as the minimum pulse width. This is the typically expected behavior of a Q-switched laser, and can be clearly seen to occur in Fig. 7 as the pump power is increased.

Figure 8 gives the pulse repetition rate and pulse width trends of the Q-switched laser at different pump powers. At the threshold pump power, the Q-switched output has a repetition rate of ~27.52 kHz and a pulse width of 4.16 μs. As the pump power increases, the repetition rate

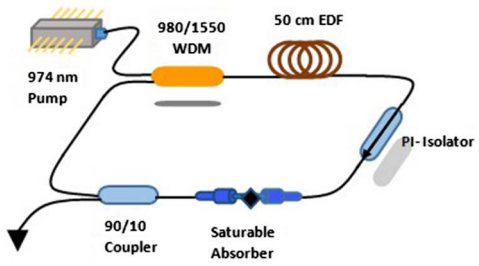

Fig. 5. Experimental setup of the C-band Q-switched EDFL with a mechanical exfoliated WSSe as an SA.

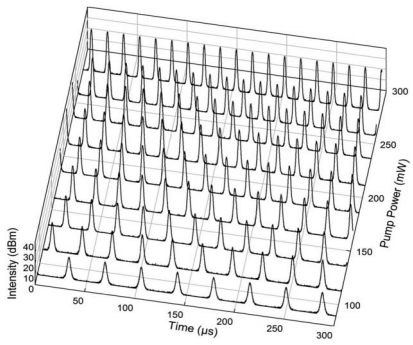

Fig. 7. 3D pulse train evolution of the proposed EDFL against the pump power.

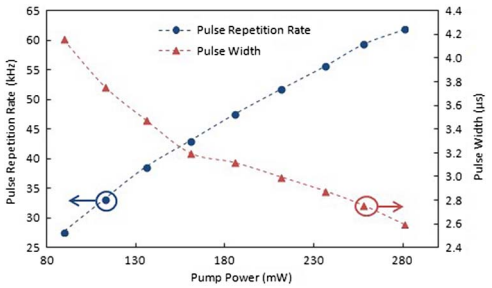

Fig. 8. Pulse repetition rate and pulse width of the Q-switched EDFL against the pump power.

increases as well, while the pulse width decreases, reaching a maximum repetition rate of 61.81 kHz and a minimum pulse width of 2.6 μs at the maximum pump power. It is also observed that while the repetition rate increases almost linearly as expected, the pulse width on the other hand shows a linear decrease, whereas it would decrease exponentially in a typical Q-switched laser. This, however, can be attributed to the SA being far from saturation, and as such the linear decrease in the pulse width is characteristic of its early behavior in a typical Q-switched laser.

As well as the pulse width and repetition rate, the output power and pulse energy of Q-switched pulses are also analyzed. The trends of these two parameters over a pump power range of 89.07 mW to 280.5 mW are given in Fig. 9. From the figure, it can be seen immediately that both the average output power and the pulse energy increase linearly against the pump power, rising from minimum values of 0.12 mW and 4.23 nJ at the threshold power to maximum values of 0.45 mW and 7.31 nJ, respectively, at the maximum pump power. The slight decrease in the pulse energy at the maximum pump power is a result of the interaction between the pulse width and the average pump power. The power conversion efficiency of the proposed laser cavity is achieved at ∼0.17%.

Stability analysis was also carried out using a radio frequency spectrum analyzer. Measurement in the small frequency range shows a highly stable radio frequency signal with a fundamental frequency of ∼61.81 kHz, as shown in Fig. 10. The stability of this signal is confirmed by the high signal-to-noise ratio (SNR) of approximately 57.8 dB as well as the absence of other frequency modes over a wider span of ∼450 kHz, as depicted by the inset

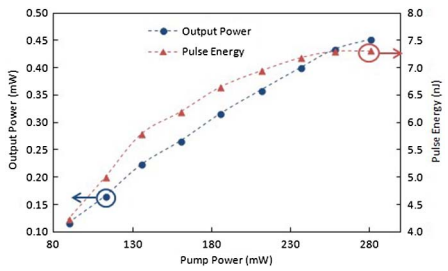

Fig. 9. Output power and pulse energy of the Q-switched EDFL against the pump power.

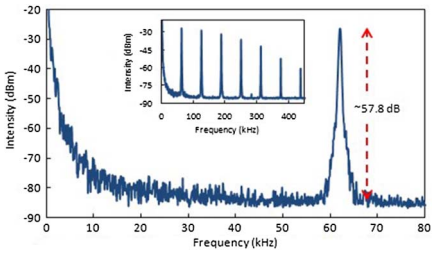

Fig. 10. Radio frequency spectrum of the Q-switched YDFL at a pump power of 280.5 mW.

of the figure. The power conversion efficiency of the proposed laser cavity achieves ∼0.17%. The low efficiency of the laser cavity is caused by the optical components loss, splicing loss between the single-mode fiber and EDF, and the low ratio of the tapped output signal. Furthermore, the insertion loss by the WSSe-based SA is about 6 dBm, which further affects the efficiency of the laser cavity. However, the conversion efficiency is comparable to other passively Q-switched laser works[15–17].

The tunability of the proposed Q-switched laser is investigated by incorporating a tunable bandpass filter (TBPF) into the cavity as a tuning element. Using the TBPF, the lasing Q-switched wavelength of the laser cavity could be tuned over a range of 1530 nm to 1570 nm, as shown in Fig. 11. Throughout the entire tuning range, a stable Q-switching is observed with only

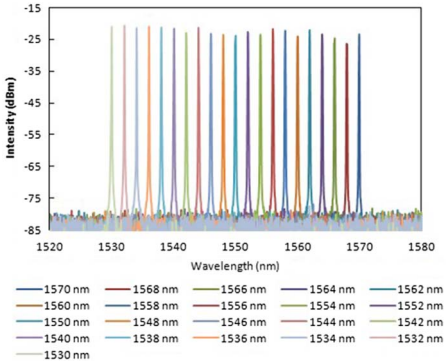

Fig. 11. Optical spectra of the tunable wavelength Q-switched laser at a maximum pump power of 280.5 mW.

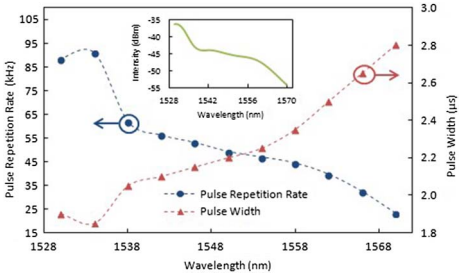

Fig. 12. Pulse repetition rate and pulse width evolution of the proposed tunable Q-switched fiber laser at the maximum pump power of 280.5 mW.

Table 1. Comparison of the Output Performance of C-band *Q*-switched Lasers Generated by Different SAs

Saturable Absorber	Operating Power (mW)	Pulse Repetition Rate (kHz)	Pulse Width (μs)	Refs.
Carbon nanotube	12.8-40.95	27.5 (max)	15 (min)	[18]
Graphene/ PVA	101.8-230.4	21.5-36.3	7.2-3.2	[19]
MoS_2/PVA	18.9-227.1	8.77-43.47	26.7-3.3	[20]
WS_2/PVA	60-300	4.5-49.6	7.9-3.1	[21]
$MoSe_2$/PVA	22.4-102.0	16.9-32.8	59.1-30.4	[2]
Bi_2Te_3-graphene	59.9-304	9.3-35.07	23-3.247	[22]
WSSe	89.07-280.5	27.52-61.81	4.16-2.6	This work

minor fluctuations in the output power. However, no *Q*-switched lasing is observed beyond the aforementioned wavelength range due to insufficient gain in the laser cavity to promote the saturation required for *Q*-switching operation.

Figure 12 shows the repetition rate and pulse width of the *Q*-switched laser output over the same wavelength tuning range. Tuning of the central wavelength from 1530 nm to 1570 nm sees the pulse repetition rate of the *Q*-switched laser decrease from 88.50 to 23.26 kHz whereas the pulse width increases from 1.9 μs to 2.8 μs. This behavior corresponds well with the gain profile of the EDF over the 40 nm tuning range.

The proposed laser of this work is capable of generating highly stable *Q*-switched outputs over a wide tuning range of ~40 nm with a high SNR of ~57.8 dB. Significant improvement in terms of *Q*-switching output has also been observed in the proposed laser cavity, where the incorporated WSSe-based SA is able to generate *Q*-switched pulses with a higher pulse repetition rate and a narrower pulse width as compared to that of other 2D materials. A comparison of the output performance of the *Q*-switched laser against other similar systems using different SAs is given in Table. 1.

In conclusion, a passive *Q*-switched EDFL operating in the C-band region has been proposed and demonstrated with the use of a WSSe-based SA. The laser has a central wavelength of ~1558.4 nm and, at the highest pump power of 280.5 mW, a maximum repetition rate of 61.81 kHz, a minimum pulse width of 2.6 μs, the highest output power of 0.45 mW, and the highest pulse energy of 7.31 nJ are achieved. Moreover, the *Q*-switched lasing output generated from the proposed laser cavity can be tuned over a broad range of ~40 nm, from 1530 nm to 1570 nm, with high stability, giving it significant potential for a variety of photonic applications.

This work was supported by the Ministry of Higher Education, Malaysia (Grant No. LRGS (2015) NGOD / UM / KPT) and the University of Malaya (Grant Nos. RU 001-2017 and RP 029A –15 AFR).

References

1. H. Ahmad, F. D. Muhammad, M. Z. Zulkifli, and S. W. Harun, J. Mod. Opt. **60**, 1563 (2013).
2. H. Ahmad, M. Suthaskumar, Z. C. Tiu, A. Zarei, and S. W. Harun, Opt. Laser Technol. **79**, 20 (2016).
3. F. D'Apuzzo, A. Di Gaspare, V. Giliberti, O. Limaj, P. Roy, M. Brahlek, N. Koirala, S. Oh, F. J. García de Abajo, and S. Lupi, Adv. Opt. Mater. **3**, 1257 (2015).
4. S. Tani, F. Blanchard, and K. Tanaka, Phys. Rev. Lett. **109**, 166603 (2012).
5. A. Kumar and P. K. Ahluwalia, Eur. Phys. J. B **85**, 186 (2012).
6. H. Li, G. Lu, Y. Wang, Z. Yin, C. Cong, Q. He, L. Wang, F. Ding, T. Yu, and H. Zhang, Small **9**, 1974 (2013).
7. S. Horzum, H. Sahin, S. Cahangirov, P. Cudazzo, A. Rubio, T. Serin, and F. M. Peeters, Phys. Rev. B **87**, 125415 (2013).
8. X. Duan, C. Wang, Z. Fan, G. Hao, L. Kou, U. Halim, H. Li, X. Wu, Y. Wang, and J. Jiang, Nano Lett. **16**, 264 (2016).
9. J. Kang, S. Tongay, J. Li, and J. Wu, J. Appl. Phys. **113**, 143703 (2013).
10. H. Ahmad, S. A. Reduan, S. N. Aidit, and Z. C. Tiu, Chin. Opt. Lett. **15**, 020601 (2017).
11. J. Shakya, S. Kumar, D. Kanjilal, and T. Mohanty, Sci. Rep. **7**, 9576 (2017).
12. H. Zeng, G.-B. Liu, J. Dai, Y. Yan, B. Zhu, R. He, L. Xie, S. Xu, X. Chen, and W. Yao, Sci. Rep. **3**, 1608 (2013).
13. Y. Cui, F. Lu, and X. Liu, Sci. Rep. **6**, 30524 (2016).
14. M. Chernysheva, C. Mou, R. Arif, M. AlAraimi, M. Rümmeli, S. Turitsyn, and A. Rozhin, Sci. Rep. **6**, 24220 (2016).
15. H. Ahmad, N. E. Ruslan, M. A. Ismail, Z. A. Ali, S. A. Reduan, C. S. J. Lee, and S. W. Harun, Laser Phys. **26**, 095103 (2016).
16. H. Ahmad, N. E. Ruslan, M. A. Ismail, S. A. Reduan, C. S. J. Lee, S. Sathiyan, S. Sivabalan, and S. W. Harun, Appl. Opt. **55**, 1001 (2016).
17. H. Ahmad, A. Z. Zulkifli, Y. Y. Kiat, and S. W. Harun, Opt. Commun. **310**, 53 (2014).
18. B. Dong, J. Hu, C.-Y. Liaw, J. Hao, and C. Yu, Appl. Opt. **50**, 1442 (2011).
19. H. Ahmad, S. A. Reduan, N. A. Hassan, S. I. Ooi, and Z. C. Tiu, Laser Phys. **27**, 075103 (2017).
20. Y. Huang, Z. Luo, Y. Li, M. Zhong, B. Xu, K. Che, H. Xu, Z. Cai, J. Peng, and J. Weng, Opt. Express **22**, 25258 (2014).
21. B. Chen, X. Zhang, C. Guo, K. Wu, J. Chen, and J. Wang, Opt. Eng. **55**, 081306 (2016).
22. H. Mu, Z. Wang, J. Yuan, S. Xiao, C. Chen, Y. Chen, Y. Chen, J. Song, Y. Wang, and Y. Xue, ACS Photonics **2**, 832 (2015).